Spine Deformity

www.spine-deformity.org

Spine Deformity 5 (2017) 197–207

Sequential Magnetic Resonance Imaging Reveals Individual Level Deformities of Vertebrae and Discs in the Growing Scoliotic Spine

Bethany E. Keenan, PhD[a,*], Maree T. Izatt, BPhty[a], Geoffrey N. Askin, FRACS[a], Robert D. Labrom, FRACS[a], Damon D. Bennett, MAppSc[b], Mark J. Pearcy, DEng[a], Clayton J. Adam, PhD[a]

[a]*Paediatric Spine Research Group, Queensland University of Technology and Mater Health Services Brisbane Ltd, Level 5, Centre for Children's Health Research, 62 Graham St, South Brisbane, Q4104,, Australia*

[b]*MRI Department, Mater Health Services, Raymond Terrace, South Brisbane, Q4104, Australia*

Received 28 July 2015; revised 28 September 2016; accepted 4 October 2016

Abstract

Study Design: The aim of this study was to measure contributions of individual vertebra and disc wedging to coronal Cobb angle in the growing scoliotic spine using sequential magnetic resonance imaging (MRI). Clinically, the Cobb angle measures the overall curve in the coronal plane but does not measure individual vertebra and disc wedging. It was hypothesized that patients whose deformity progresses will have different patterns of coronal wedging in vertebrae and discs to those of patients whose deformities remain stable.

Methods: A group of adolescent idiopathic scoliosis (AIS) patients each received two to four MRI scans (spaced 3–12 months apart). The coronal plane wedge angles of each vertebra and disc in the major curve were measured for each scan, and the proportions and patterns of wedging in vertebrae and discs were analyzed for subgroups of patients whose spinal deformity did and did not progress during the study period.

Results: Sixteen patients were included in the study; the mean patient age was 12.9 years (standard deviation 1.7 years). All patients were classified as right-sided major thoracic Lenke Type 1 curves (9 type 1A, 4 type 1B, and 3 type 1C). Cobb angle progression of ⩾5° between scans was seen in 56% of patients. Although there were measurable changes in the wedging of individual vertebrae and discs in all patients, there was no consistent pattern of deformity progression between patients who progressed and those who did not. The patterns of progression found in this study did not support the hypothesis of wedging commencing in the discs and then transferring to the vertebrae.

Conclusion: Sequential MRI data showed complex patterns of deformity progression. Changes to the wedging of individual vertebrae and discs may occur in patients who have no increase in Cobb angle; therefore, the Cobb method alone may be insufficient to capture the complex mechanisms of deformity progression.

Keywords: Adolescent idiopathic scoliosis; Cobb angle; Magnetic resonance imaging; Curve progression; Spine deformity

Introduction

Adolescent idiopathic scoliosis (AIS) is a complex deformity of the spinal column and trunk for which the cause has not yet been identified. A key problem with the assessment and treatment of scoliosis is the current lack of understanding of the mechanisms governing deformity progression. In current clinical practice, scoliosis severity and progression is assessed through repeated radiographic measurements of the Cobb angle, a single angle that describes the severity of the lateral scoliotic curve (usually containing 6–8 intervertebral joints) on coronal plane standing radiographs [1]. However, the use of clinical radiographs in exploring underlying patterns of deformity progression during growth is not desirable, because they involve repeated exposure to ionizing radiation and suffer from poor contrast when imaging soft tissues. The combined dose for full spine posteroanterior (PA) and lateral standing radiographs is in the order of 1.0 mSv, and the annual background radiation in Queensland, Australia, is approximately 2.0–2.4 mSv [2,3]. Patients diagnosed with AIS have historically undergone an average of 12 to 22

Author disclosures: BEK (none); MTI (none); GNA (none), RDL (none); DDB (none); MJP (none); CJA (none).

*Corresponding author. Room S2.39 School of Engineering, Cardiff University, Queen's Buildings, 14-17 The Parade, Cardiff, CF24 3AA, Wales, United Kingdom. Tel: (+44) 2920 687 650; fax: (+44) 2920 874 939.

E-mail address: keenanb@cardiff.ac.uk (B.E. Keenan).

2212-134X/$ - see front matter © 2016 Scoliosis Research Society. All rights reserved.
http://dx.doi.org/10.1016/j.jspd.2016.10.002

plain radiographs during a 3-year surveillance period, exposing the patient to significant levels of radiation [4,5], which in the modern era is being reduced as alternative surveillance and imaging techniques are developed. Nonionizing imaging modalities such as magnetic resonance imaging (MRI) are favorable, but are currently only used routinely for preoperative AIS patients to detect suspected intracranial and intraspinal anatomic or neurologic abnormalities rather than for assessment of the deformity itself.

When studying the progression of scoliotic deformities during skeletal growth, it is imperative to explore changes occurring at the level of individual vertebrae and discs (ie, not just the overall Cobb angle), because the degree of local deformity varies with location in the major scoliotic curve [6-8], and the biomechanical forces driving deformity progression are also not uniformly distributed within the major curve [9].

Several previous studies have suggested that there is a relationship between vertebral wedging and spinal growth in scoliosis, and that wedging initiates in the discs and later in the vertebrae [6,8,10,11]. Vertebral wedging and scoliosis progression have been reported in both mild and moderate curves, with wedging increasing primarily in the three levels inferior to the curve apex [7].

With the increasing awareness surrounding radiation doses in children, and the strong relationship of scoliosis curve progression with growth, it is important to assess the growing scoliotic spine with a nonionizing imaging modality. For this reason, the aims of this study were (1) to measure the individual deformations of the vertebrae and discs in the growing scoliotic spine using sequential MRI; (2) to examine the differences at the vertebra/disc level between those patients whose curve progressed and those whose did not; and (3) to consider the clinical implications of these findings.

Since the coronal plane Cobb angle is the current standard for clinical assessment of scoliosis progression, this study looked at the wedging and height changes of the vertebrae and discs only in the coronal plane. It was hypothesized that there is a consistent pattern of increasing coronal plane deformity in the vertebrae and discs with curve progression during growth, and that this pattern will differ between patients whose deformity progresses and those whose does not.

Methods

MRI protocol

A 3D MRI protocol was developed using a 3-Tesla (3T) MRI scanner (Philips Achieva 3.0T TX Dual Transit system, Amsterdam, Netherlands) at the Mater Hospital, Brisbane, Australia. A coronal ''scout'' image stack (a low-resolution scan containing 9–10 slices) was taken to capture the whole spine and identify the major scoliotic curve. The protocol used to perform the scout scan was a T_1-weighted 2D gradient echo sequence with an acquisition time of 5 minutes. The time to repetition (TR) and the time to echo (TE) were set as 6.9 and 4.6 milliseconds, respectively, with a flip angle of 20°. The protocol for the high-resolution 3D scan of the major scoliotic curve was a T_1-weighted 3D gradient echo sequence, with an isotropic voxel size of 0.49 mm, TR of 5.9 milliseconds, TE of 2.7 milliseconds, flip angle of 5°, and an acquisition time of 15 minutes. The field of view was adjusted according to the patient's deformity to ensure the whole of the major curve was captured. The 3D volume acquired using this sequence was 250 × 250 × 95 mm. Patients were in the supine position with arms by their side for all scans.

Patient demographics and clinical data collection

MRI scans were obtained for a group of AIS patients from the Mater Children's Hospital Spinal Clinic in Brisbane, Australia, over a 14-month period. Standing coronal Cobb angle and Risser Grade [12] were assessed on each patient's clinical standing radiograph, at routine spine clinic appointments, usually within a month of the MRI scan date. Standing height, rib hump, and menarche status were recorded from the patient's spine clinic records. Suitable patients were identified as those who had been diagnosed with AIS, aged a minimum of 10 years (to the nearest 0.1 year). Participants' clinical care was not altered as a result of their participation in the project and therefore could be either braced or unbraced, but never having received operative treatment. As our Center draws patients from a large geographical area, patients also had to be willing to commit to attend our Center for the research scans and travel the sometimes long distances that were involved to participate. As the primary focus was on curve progression during the adolescent growth phase, only patients who were Risser grade <3 were included, to ensure there was still remaining spine growth until skeletal maturity. Leg length differences of up to 1 cm were considered acceptable. Patients underwent an initial MRI scan after recruitment to the study, then received up to three more scans during growth until they either went on to surgery or were discharged from the clinic.

To capture the rapid growth spurt of the patient, the time periods between the scans varied according to the stage of growth of individual patients, determined during their clinical appointments with the spinal orthopaedic surgeons as part of their standard care. Informed consent was received from all participants and parents, and ethical approvals were obtained from the Mater Human Research Ethics Committee and Queensland University of Technology Human Research Ethics Committee.

Image analysis

To assess the change in coronal plane deformity during the adolescent growth phase, the MRI scans for each patient

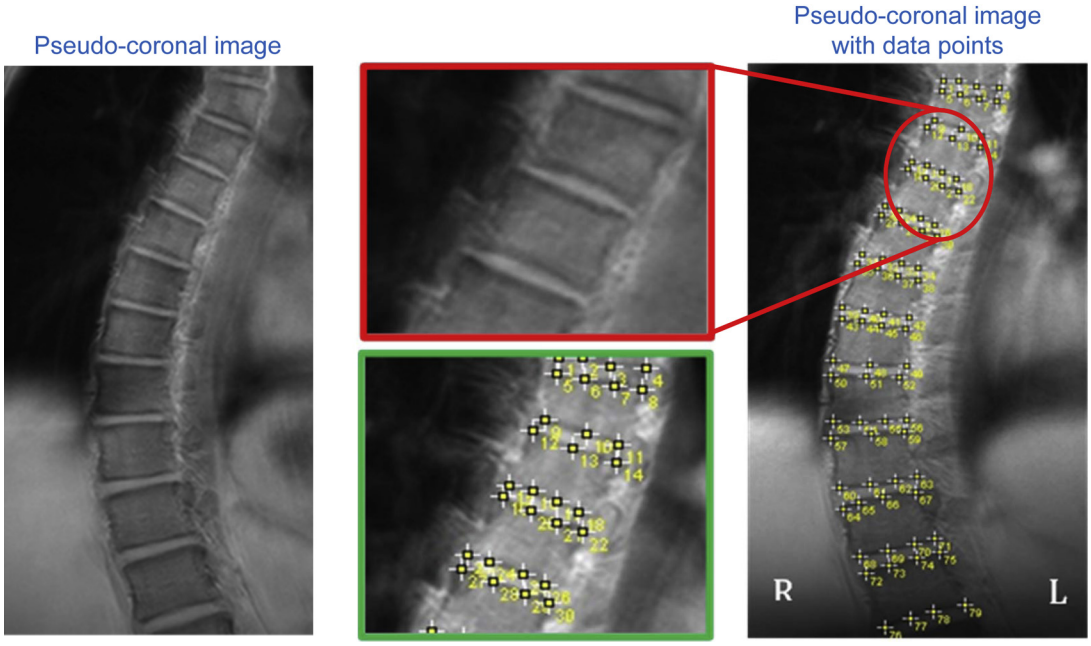

Fig. 1. Z-project (pseudo-coronal image) of major coronal curve showing selected (convex to concave) data points manually selected along the superior and inferior endplates. Red circle illustrates the endplate curvature where the disc space is narrowed toward the edges of the disc.

were manipulated using image-processing software, ImageJ (v. 1.45, National Institutes of Health, Bethesda, MD). To measure coronal plane wedging of vertebrae and discs in the major scoliotic curve, 2D coronal projections were generated from the 3D MRI data set as described below.

The Z-project function in ImageJ allowed the coronal slices within the stack to be combined to produce a pseudo-coronal projection [13,14] such that all vertebrae and discs within the major curve were visible on a single 2D image (Fig. 1). The Z-project function can be applied on selected slices within the stack so only the region of stack thickness of interest is displayed. For this study, the anterior and posterior edges of each vertebral body were selected within the stack to project a clear image of the major curve in the anterior vertebral column (without the posterior elements or ribs).

The projection type ‘‘sum slices’’ was found to give the clearest visualisation of the vertebral endplates. The sum slices projection implements

$$o_{x,y} = \sum_{s=\text{anterior}}^{\text{posterior}} i_{x,y},$$

where o is the intensity of the projected image pixel at location x, y in the output image, and i is the intensity of the input image pixel at the same x, y location on slice s. The summation is performed across all slices between anterior and posterior vertebral column boundaries.

The next step was to segment the inferior and superior endplates for each vertebra in the major curve from the pseudo-coronal image. The ‘‘multi-point’’ tool in ImageJ was used to manually select three to four points along each vertebral endplate (from the convex to concave side of the major scoliotic curve) to capture the profile of each endplate (Fig. 1). The coronal plane image co-ordinates of each data point of all the vertebral levels in the major curve were then exported to Excel for analysis.

Calculating vertebral and disc wedging

The coronal plane wedge angle between pairs of adjacent endplates (either encapsulating an intervertebral disc or a vertebral body) were found using the LINEST function in Excel. This function allowed a line of best fit to be calculated through the data points of each endplate from which the difference between the angles of adjacent pairs of endplates gave the coronal plane wedge angle in the vertebrae and discs. By convention, positive wedge angles were defined as those with the same sense as the major curve (eg, for a right thoracic major curve, individual vertebra and disc wedge angles were positive when the wedge was open toward the convexity of the major curve). However, negative wedge angles also occur in scoliotic curves, in which the wedge of a vertebra or disc is directed in the opposite sense to the major curve wedging. Fig. 2 shows a schematic representation of a portion of a scoliotic curve showing both positive and negative vertebral body (VB) and intervertebral disc (IVD) wedging angles.

Having measured the wedge angles for all vertebrae and discs in the MR scan field of view, the major curve extents were defined according to the Cobb method. The total percentage of wedging in vertebrae and discs in the major

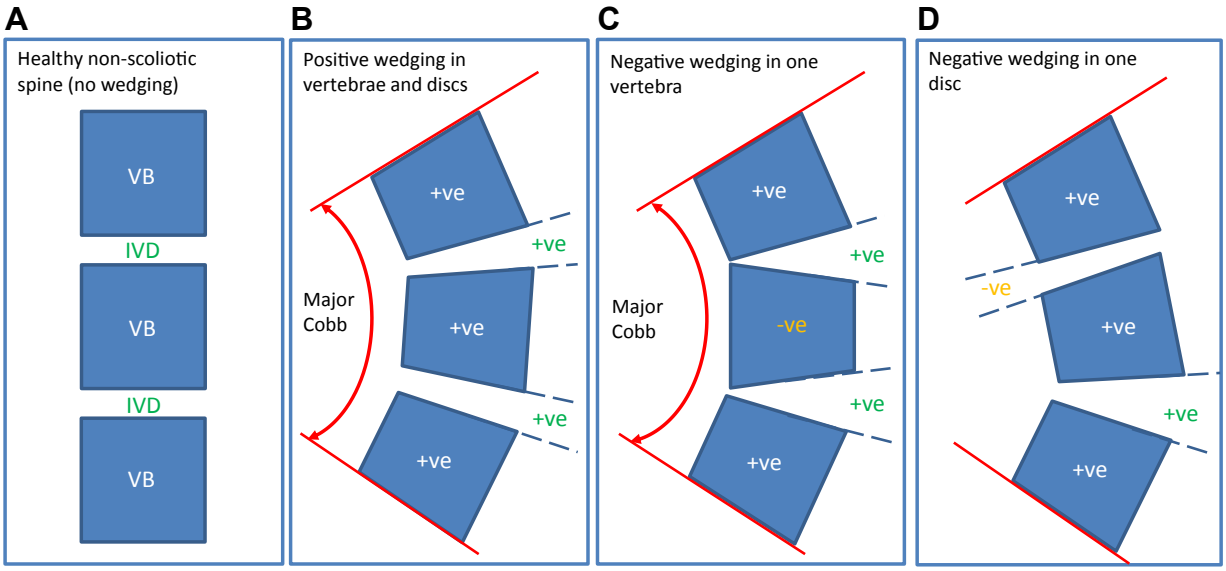

Fig. 2. Schematic of the different cases of wedging that occurred in the discs or vertebrae, where (A) healthy spine (non-scoliotic); (B) typical scoliotic curve with positive wedging in both vertebrae and discs; (C) scoliotic curve with one negatively wedged vertebra; and (D) scoliotic curve with one negatively wedged disc. Note: +ve refers to positive wedging (toward the curve convexity) and −ve refers to negative wedging (towards the concave side of the curve).

curve was then calculated by summing the individual wedge angle contributions of all the IVDs and VBs, respectively, in a particular scoliotic curve. Coronal plane wedging results were also expressed by dividing the major scoliotic curve into two regions, above the apex (AA) and below the apex (BA), in order to assess whether more wedging occurred above or below the apical vertebra. The apical level was chosen from each MRI scan's coronal projection. If the apical location was a disc, then for the purposes of the present study, the adjacent superior vertebra was chosen. The wedging in the apical vertebra was then shared equally between AA and BA (Fig. 3).

Intraobserver variability

Intraobserver variability for the individual endplate tilt angle (α) was assessed through repeat measurements by a single observer using Equation 1,

$$\triangle \alpha = |\alpha_n - \alpha_n + 1|, \quad (1)$$

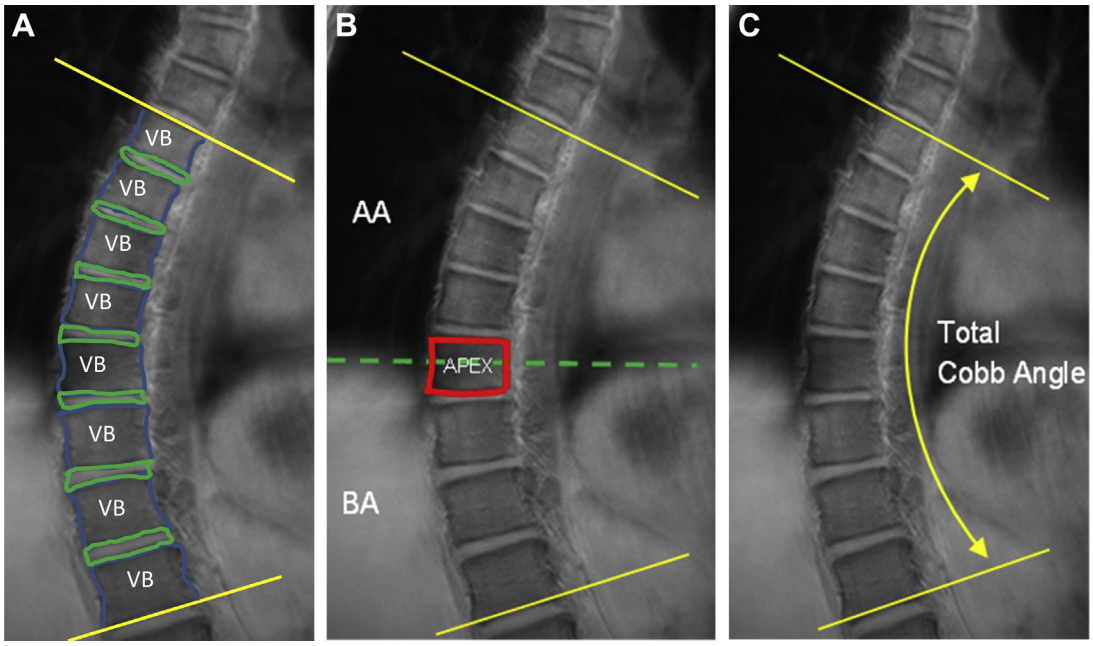

Fig. 3. The three levels of assessment for the major curve. (A) Individual vertebral bodies (VBs) (blue) and intervertebral discs (IVDs) (green) in the major curve. (B) The percentage of Cobb angle above apex (AA) and below the apex (BA) and (C) the overall Cobb angle.

where n and $n + 1$ are successive measurements. The mean signed intraobserver difference was −0.1°, which is not significantly different from zero and suggests that no order bias existed between the first and second measurements. Mean absolute (unsigned) intraobserver difference was 2.5°, the standard deviation of the difference was 2.0°, and the 95% limits of agreement (1.96 × standard deviation) were ±3.9°.

Analysis of deformity progression

For the purposes of assessing patterns of progression, the patient group was then divided into two categories, those whose deformity progressed during the study time period and those whose did not. To avoid confusion in the presentation of results, the term *Interval* here refers to the time period between any two MRI scans for a particular patient. For example: three MRI scans were performed on Patient 1; therefore, there are three possible intervals: between Scan 1 and Scan 2 (1–2), between Scan 2 and Scan 3 (2–3), and between Scan 1 and Scan 3 (1–3) for this patient.

Progression of the deformity was deemed to have occurred if the Cobb angle increased by the value used clinically of 5° or more. For example, if a patient had a major Cobb angle of 30° at Scan 1, 34° at Scan 2, and 40° at Scan 3, then his or her curve was seen to progress over intervals 2–3 and 1–3. Therefore, this patient would have been categorized in the ''Progressed'' group. To look for patient variables that were predictive of progression over an interval between scans, a multiple regression analysis was performed across all intervals in the study, with Cobb change over the interval as the dependent variable and the following five candidate independent variables: (1) length of interval; (2) age at start of interval; (3) major Cobb at start of interval; (4) percentage of major curve wedging in discs at start of interval; and (5) whether the patient was braced during the interval (0 = no, 1 = yes).

Results

Patient demographics and height growth

Twenty-one patients were recruited to the study; however, five of these patients were later excluded. One patient failed to complete the first scan because of claustrophobia, one was unable to lie sufficiently still during scanning, one was lost to clinical follow-up with no explanation, one was excluded on the basis of having a left thoracolumbar major curve, and one was excluded due to being later reclassified as Risser 4 (having originally been incorrectly classified as Risser 2). Of the remaining 16 patients, the mean age at recruitment was 12.9 years (standard deviation 1.7 years) and all curves were right-sided major thoracic Lenke Type 1, with 9 patients classified as lumbar spine modifier A, 4 as lumbar modifier B, and 3 as lumbar modifier C [15]. No patient had a leg length discrepancy more than 1 cm. Risser grades at the start of the first scan ranged from 0 to 2 (as per the inclusion criteria), with 10 patients classified Risser 0, three as Risser 1, and three as Risser 2.

Table 1 shows the patient demographics (age, maturity, height and curve classification) for each patient at commencement of the study, where their Risser grade and

Table 1
Clinically measured age, maturity, and curve classification for each patient at the commencement of the study (n = 16).

Patient	Age (year)	Menarche age (years)	Risser grade (0–5)	Lenke class	Standing height (cm)	Braced?
1	14.2	13.1	2	1C	163	
2	16.0	Pre	0	1A	162	Y
3	11.3	Pre	0	1A	149	Y
4	13.9	12.7	1	1A	165	Y
5	11.9	11.6	1	1A	151	Y[a]
6	13.0	Pre	0	1A	155	Y
7	14.4	14.0	2	1B	168	
8	14.3	Pre	0	1C	170	Y
9	14.6	13.8	2	1B	153	Y[a]
10	11.6	Pre	0	1B	152	Y
11	13.9	13.9	1	1A	163	Y
12	11.2	Pre	0	1A	136	Y
13	12.9	Pre	0	1C	145	Y
14	10.6	Pre	0	1A	134	
15	10.0	Pre	0	1A	135	
16	12.4	Pre	0	1B	144	
Mean	12.9				153	

Risser grade and Lenke classification were assessed on each patient's first clinical standing radiograph.

[a] Patients 5 and 9 were not braced at the commencement of the study but received a brace between the first and second scans.

Table 2
Standing heights measured at the time of each MRI scan.

Patient	Scan 1	Scan 2	Scan 3	Scan 4
1	162.7	162.9 (+0.2)	162.9 (+0.2)	
2	162.4	—[a]	—[a]	
3	148.5	152.0 (+3.5)	152.0 (+3.5)	
4	164.5	166.2 (+1.7)	166.5 (+2.0)	
5	151.3	156.2 (+4.9)	159.0 (+7.7)	160.5 (+9.2)
6	155.3	159.0 (+3.7)	164.0 (+8.7)	164.5 (+9.2)
7	168.0	168.3 (+0.3)		
8	170.3	173.0 (+2.7)	174.5 (+4.2)	
9	153.0	153.5 (+0.5)	155.0 (+2.0)	
10	152.0	154.0 (+2.0)	155.0 (+3.0)	
11	163.3	166.0 (+2.7)	166.5 (+3.2)	
12	136.3	144.0 (+7.7)		
13	145.2	155.0 (+9.8)		
14	133.6	144.5 (+10.9)		
15	134.5	146.0 (+11.5)		
16	144.0	154.0 (+10.0)		

MRI, magnetic resonance imaging.

All measurements are in centimeters. Growth relative to the first scan is given in parentheses.

[a] Note that no height measurement data were available for Patient 2 subsequent to the initial scan.

Table 3
Major curve levels measured from each MRI scan (n = 16).

Patient	Scan 1	Scan 2	Scan 3	Scan 4
1	T6–L1	T6–L1	T6–L1	
2	T4–T11	T4–T12[a]	T4–T11[a]	
3	T6–L1	T6–L1	T6–L1	
4	T6–L1	T5[a]–L1	T6[a]–L1	
5	T5–T11	T4[a]–T11	T4–T11	T5[a]–T12[a]
6	T6–T11	T6–T11	T6–T11	T5[a]–T11
7	T5–T12	T6[a]–T12		
8	T5–T11	T5–T11	T5–T11	
9	T5–L1	T5–T12[a]	T6[a]–T12	
10	T4–T11	T4–T12[a]	T4–T11[a]	
11	T5–T11	T5–T10[a]	T5–T10	
12	T6–T11	T6–T10[a]		
13	T5–T10	T4[a]–T10		
14	T4–T12	T4–L1[a]		
15	T5–T9	T5–T11[a]		
16	T5–T10	T6[a]–T10		

MRI, magnetic resonance imaging.
[a] Change in the curve extent relative to the previous scan.

Lenke type were assessed from their clinical standing radiographs. Table 1 also indicates those patients who were braced during the study. Nine (56%) of the 16 patients were braced at the time of the first scan, with two further patients (Patients 5 and 9) receiving brace treatment between Scans 1 and 2. Subsequent to the study, six patients (Patients 1, 3, 5, 10, 12, and 13) went on to receive surgery, three patients (Patients 14, 15, and 16) are yet to reach skeletal maturity so are still under clinical observation, and seven patients (Patients 2, 4, 6, 7, 8, 9, and 11) have been discharged, being skeletally mature and not requiring surgical intervention.

Table 2 gives the standing height of each patient at each scan appointment. The heights were measured by the same nurse immediately prior to the scan using the same equipment (0.1 cm resolution) for the entire study.

Sequential scan Cobb changes and progression

Of the 16 patients analysed, six received 2 scans, eight received 3 scans and two received 4 scans, making a total of 42 intervals between scans (16 scans 1–2 intervals, 10 scans 2–3 intervals, 10 scans 1–3 intervals, 2 scans 2–4 intervals, 2 scans 3–4 intervals, and 2 scans 1–4 intervals).

Table 3 shows the major curve levels for each patient across the series of scans, as measured on the supine MRI scans themselves. Fig. 4 shows the major thoracic supine Cobb angles of each patient in the study (n = 16), where the markers indicate individual scans for a particular patient. Table 4 shows the Cobb angle changes (with progression of 5° or more shaded in gray) that occurred over each interval for each patient in the study, including an indication of how much of the progression occurred in the vertebral bodies and discs, respectively. Overall, 9 of the 16 patients progressed, and progression of 5° or more occurred in 19 of the 42 intervals (45%) in the study.

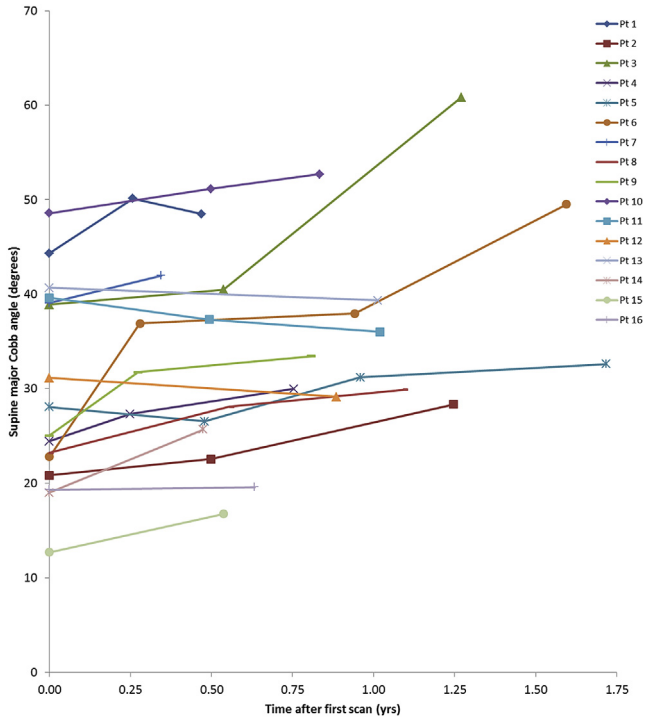

Fig. 4. A line graph of the coronal plane major Cobb angle versus time after the first scan for all 16 patients in the study, with markers indicating a particular scan and lines connecting pairs of sequential scans.

The multiple regression analysis revealed a statistically significant direct relationship between major Cobb change over an interval and interval length (p = .04), but none of the other candidate independent variables were statistically significant. Fig. 5 shows a scatter plot of interval length versus Cobb angle change during the interval, separated into two series: patients who progressed and those who did not.

Relative contributions of wedging in vertebrae and discs

The relative contributions to the overall coronal plane wedging by vertebral bodies and intervertebral discs for each patient are shown in Fig. 6. In 7 of the 16 patients in this graph (Patients 2, 4, 8, 10, 12, 14, and 16), the deformity at Scan 1 occurs predominantly (>50% of total Cobb angle) in the discs. In four (Patients 2, 8, 12, and 16) of these seven patients, the initial scan is followed by a shift toward deformity predominantly (>50%) occurring in the vertebral bodies. In the other three patients (Patients 4, 10, and 14), the deformity remains primarily in the discs throughout the scanning sequence. For the other nine patients in the study (Patients 1, 3, 5, 6, 7, 9, 11, 13, and 15), deformity commences primarily (>50%) in the vertebral bodies and

Table 4
Major Cobb angle changes (in degrees) for all intervals in the study, together with height growth velocity over the interval.

Patient	Interval 1–2				Interval 2–3				Interval 3–4				Interval 1–3				Interval 2–4				Interval 1–4				Progressed
	Total	IVDs	VBs	GV	Total	IVDs	VBs	GV	Total	IVDs	VBs	GV	Total	IVDs	VBs	GV	Total	IVDs	VBs	GV	Total	IVDs	VBs	GV	
1	**6**	3	3	0.1	**−2**	0	−2	0.0					**4**	3	1	0.0									Y
2	**2**	−9	11		**6**	2	3						**8**	−7	15										Y
3	**2**	−10	12	0.5	**20**	28	−7	0.0					**22**	17	5	0.2									Y
4	**3**	−3	6	0.6	**3**	11	−8	0.5					**6**	8	−2	0.2									Y
5	**−2**	−1	−1	0.9	**5**	9	−4	0.6	**1**	−2	4	0.2	**3**	8	−5	0.7	**6**	7	−1	0.3	**5**	6	−2	0.4	Y
6	**14**	14	0	1.1	**1**	−4	5		**12**	−1	13	0.1	**15**	10	5	0.8	**13**	−5	18	0.3	**27**	9	18	0.5	Y
7	**3**	9	−7	0.1				0.2																	
8	**5**	4	1	0.4	**2**	−16	18	0.2					**7**	−13	19	0.3									Y
9	**5**	6	−1	0.2	**3**	−1	5	0.2					**8**	4	4	0.2									Y
10	**3**	−12	14	0.3	**2**	17	−15	0.1					**4**	5	−1	0.3									
11	**−2**	11	−12	0.5	**−3**	−8	5						**−5**	3	−7	0.3									
12	**−2**	−12	10	0.7																					
13	**−1**	−1	0	0.8																					
14	**7**	2	4	1.9																					Y
15	**4**	21	−18	1.8																					
16	**0**	−6	6	1.3																					

GV, growth velocity (in centimeters/month); IVD, intervertebral disc; VB, vertebral body.
The total Cobb change for each interval is given in bold, followed by the summative coronal wedging changes in the discs and vertebral bodies of the major curve, respectively (again in degrees, which add to give the overall Cobb change). Intervals with major Cobb progression of 5° or more are shaded grey.

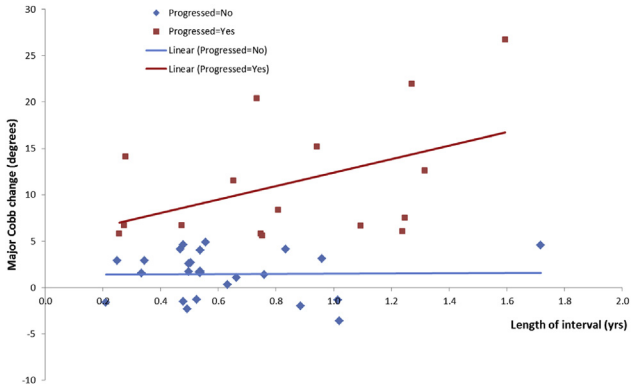

Fig. 5. Scatter plot of major Cobb angle change versus length of interval, where red markers indicate where progression (Cobb angle change ⩾5°) occurred over any interval during the study period and blue markers indicate where no progression occurred.

tends to remain at a similar proportion of total Cobb throughout the scanning sequence, with the exception of Patients 3 and 15, for whom the proportion of deformity shifted toward the discs in later scans. Patient 15 is of note because the discs were substantially negatively wedged at Scan 1 in this patient.

When considering proportions of deformity above and below the apical vertebra, the mean proportions of coronal wedge above and below the apex for the entire patient group were 57% and 43%, respectively, at the first scan, remaining virtually unaltered at 56% and 44% for the last scan. Disc wedging occurred more above the apex than below, with mean disc wedge above the apex accounting for 27% of total Cobb angle at the first scan, compared to only 15% below the apex. Again this proportion remained relatively constant throughout the study period, such that at the last scan the mean disc wedge above the apex was 28% of total Cobb, compared with 17% below the apex. Vertebral body wedging was evenly divided above and below the apex, accounting for mean 30% and 28% of total Cobb, respectively, at the first scan, and 28% and 27% at the final scan.

In terms of coronal plane wedging at individual spinal levels in individual patients, of the 604 individual vertebra and disc wedge measurements in the study, 118 of these were negatively wedged (<0°). Of these, only 8 individual levels had a greater negative wedge magnitude than the 95% intraobserver limits of agreement of 3.9°. These highly negatively wedged individual levels occurred in the T12–L1 disc of Patient 3 at Scan 3, the T5 vertebral body of Patient 5 at Scan 2, the T4 vertebrae of Patients 10 and 13 at their first scans, the T4–T5 disc and T6 vertebral body of Patient 14 at Scan 2, and the T7–T8 disc and T5–T6 disc of Patient 15 at Scans 1 and 2, respectively. Large positive wedge angles (>3.9°) occurred in 102 of the 604 individual measurements in the study, with 65 of these in vertebral bodies and 37 in discs. Individual VB and IVD wedge angles for each level in the major curve are shown for each patient in Table 5.

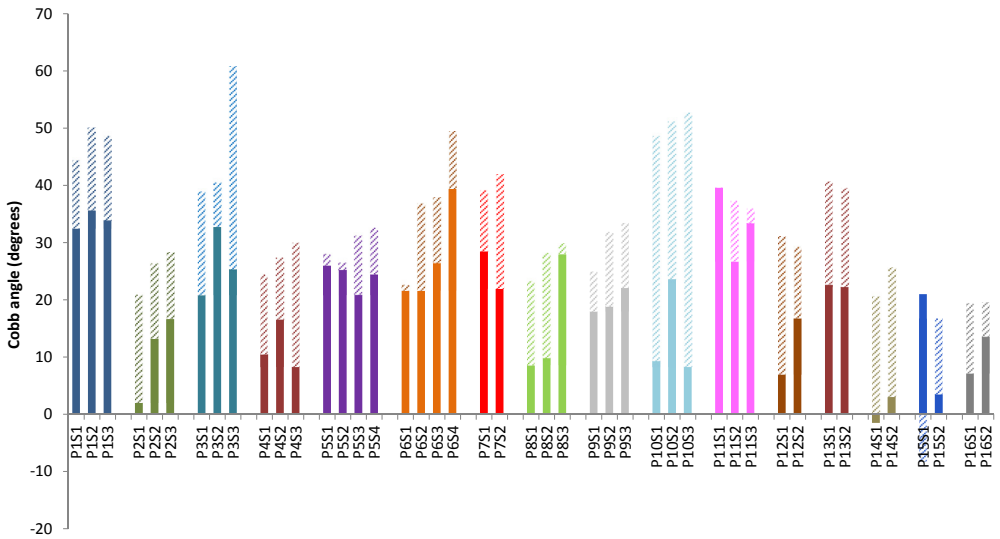

Fig. 6. Chart of Cobb angle for each patient in the study. The relative contributions of wedging in the vertebrae (solid colour) and discs (light shade) are stacked for each scan (P*x*S*y*, where *x* is patient number and *y* is scan number for that patient). Note that a negative Cobb angle indicates negative wedging, so in these cases the overall Cobb angle will be less than the height of the positive bar. For example, Patient 15 had a major Cobb angle of 13°, with 21° contribution from the vertebral body (VB) and −8° from the intervertebral discs (IVDs).

Table 5
Individual level coronal plane wedge angles for all patients and all intervals in the study.

Level	P1S1	P1S2	P1S3	P2S1	P2S2	P2S3	P3S1	P3S2	P3S3	P4S1	P4S2	P4S3	P5S1	P5S2	P5S3	P5S4	P6S1	P6S2	P6S3	P6S4	P7S1	P7S2	P8S1	P8S2	P8S3	P9S1	P9S2	P9S3	P10S1	P10S2	P10S3	P11S1	P11S2	P11S3	P12S1	P12S2	P13S1	P13S2	P14S1	P14S2	P15S1	P15S2	P16S1	P16S2
T1																																												
T1–T2																																												
T2																																												
T2–T3																																												
T3																																												
T3–T4																																												
T4				-2.4	3.6	6.5								-0.8	2.1													-4.0	7.0	-3.2								-4.1	-2.5	6.4				
T4–T5				3.3	-2.8	-2.9								1.8	0.5													9.9	0.1	4.0								5.0	5.8	-4.0				
T5				-1.0	0.2	2.8					2.9		1.6	-4.2	1.3	4.5				1.7	-0.5		3.5	-1.0	3.1	-2.6	0.9		-2.7	3.1	-3.5	8.8	5.0	-0.8			2.2	-1.4	-3.7	3.4	2.9	2.5	2.1		
T5–T6				2.7	0.8	2.0				-0.5		-0.3	0.9	0.7	1.4					-1.4	1.5		1.4	4.3	3.7	-1.8	1.3		5.8	1.7	6.8	-0.6	3.1	1.4			2.2	4.5	1.4	-1.9	-1.8	-4.5	-1.8		
T6	3.4	0.8	0.3	2.5	0.2	0.5	5.0	4.5	3.5	-1.4	0.4	1.6	0.7	7.1	3.0	3.4	1.1	-0.3	2.9	2.0	5.2	2.9	2.5	-1.3	2.1	-1.9	2.6	6.5	0.7	0.1	2.6	11.8	6.5	7.4	0.2	0.1	4.9	4.0	-1.6	-6.7	3.5	-1.0	-1.1	2.0
T6–T7	0.0	0.6	-0.7	2.4	3.4	1.6	-2.5	-2.8	13.9	3.0	0.0	2.5	5.8	-0.4	0.7	-1.4	-1.8	5.5	0.5	8.3	-2.6	4.2	2.0	7.1	4.0	-0.4	0.5	2.7	5.3	3.9	4.1	0.1	2.7	2.9	1.6	0.5	5.6	-0.5	5.5	9.3	-2.8	7.0	2.1	2.9
T7	8.2	4.2	9.7	-1.8	1.2	0.8	3.0	4.0	2.8	0.7	0.6	3.3	3.1	5.6	5.4	4.0	7.1	5.6	8.9	8.2	9.2	7.3	2.0	3.9	4.8	7.2	-1.9	-0.6	3.3	2.5	4.7	7.5	7.8	10.2	-2.8	1.0	3.2	7.3	0.7	-3.8	7.2	-1.2	1.2	1.3
T7–T8	-2.8	-1.1	-0.9	2.2	2.9	3.9	8.1	1.3	11.2	3.4	3.4	4.1	0.9	2.1	4.2	7.0	0.4	1.5	2.3	-0.3	2.7	0.5	3.8	1.8	-0.6	-1.0	1.9	2.9	3.1	3.4	9.0	1.3	2.9	-1.5	11.3	3.8	0.8	4.0	0.7	9.7	-4.4	2.8	3.7	0.7
T8	8.2	10.3	4.4	0.6	-1.3	-0.6	6.6	9.6	6.0	1.9	4.1	0.8	7.0	6.6	5.5	0.4	9.4	9.0	8.6	11.1	-1.6	1.7	1.5	4.3	5.0	1.4	0.2	2.1	5.5	9.4	1.4	5.2	3.2	10.1	-1.0	4.3	10.8	9.7	0.4	-1.2	3.4	1.5	-1.3	5.7
T8–T9	-0.9	1.0	1.5	5.1	0.8	3.1	2.5	3.3	7.3	2.6	3.6	3.1	0.4	0.0	0.1	0.6	-1.4	3.1	-0.6	-1.2	1.9	3.2	2.5	0.9	-1.6	1.1	4.6	0.0	8.4	6.7	10.8	-0.5	2.6	0.1	9.8	5.6	5.2	1.3	6.1	2.8	0.7	3.1	6.8	2.2
T9	5.7	5.2	5.4	1.4	1.2	0.7	6.4	5.0	3.9	4.7	1.6	0.6	5.6	2.3	2.1	5.8	3.5	5.2	7.6	10.5	8.9	4.7	-1.1	1.6	6.7	4.4	2.6	2.8	6.3	3.1	3.3	3.7	1.8	3.0	3.9	7.5	0.9	5.0	0.1	-1.3	4.1	-0.7	3.3	3.2
T9–T10	2.8	3.7	3.5	0.3	2.6	2.0	4.1	1.8	4.9	-1.9	0.3	3.3	-3.6	-1.5	1.0	-1.0	0.3	-0.7	3.8	1.6	0.4	6.3	2.1	4.6	-0.9	2.8	1.6	3.7	3.6	7.1	6.6	-0.1	-0.7	-0.3	3.2	2.4	4.3	2.7	-0.8	3.4		4.4	1.4	0.2
T10	3.2	6.3	7.7	1.9	5.7	4.4	1.9	4.3	-1.0	2.3	2.1	-0.1	6.0	4.5	2.1	2.6	-0.5	2.4	0.2	4.8	6.0	0.6	1.3	1.5	4.4	2.6	6.3	5.6	3.1	-0.1	5.4	2.3	3.2	2.5	4.4	3.7	0.6	1.7	3.6	2.2		0.8	2.9	1.4
T10–T11	4.8	2.6	1.8	3.0	-0.8	2.0	3.6	3.3	4.6	1.9	-1.1	4.4	-1.1	-1.6	3.1	1.1	3.6	5.8	5.6	3.1	4.9	3.6	2.8	-0.6	-2.7	1.3	0.8	0.6	3.1	4.7	3.1	-0.1			-1.7				2.5	0.6		0.4		
T11	3.2	4.5	3.4	0.8	2.2	1.5	-1.6	3.4	1.1	1.3	3.3	-1.9	2.1	4.2	-0.6	1.4	1.1	-0.4	-1.6	1.0	-0.3	4.6	-1.0	0.8	1.7	4.6	3.7	3.1	-2.8	-3.2	-2.4	0.2			2.2				0.0	-1.6		1.6		
T11–T12	5.0	5.2	6.6		2.4		3.1	-0.2	0.8	3.1	1.5	1.9				0.5					1.7	2.2				3.4	2.0	1.3		-0.1									-0.9	3.9				
T12	1.0	1.4	-0.3		0.1		-1.8	1.4	3.9	0.5	0.0	2.1				2.3					1.5	0.1				0.5	3.0	2.6		1.6									1.4	3.3				
T12–L1	2.9	2.4	2.8				-0.7	1.1	-7.2	1.9	3.5	2.4														1.8														-1.2				
L1	-0.5	2.9	3.3				1.4	0.5	5.2	0.4	1.5	1.9														1.7														2.3				
L1–L2																																												
L2																																												

Row headings PxSx represent Patient number and Scan number, respectively. All wedge angles are in degrees. Positive and negative wedge angles greater than the intra-observer measurement variability of ±3.9° are highlighted in green or red, respectively.

Discussion

The aims of this study were to measure the individual contributions of coronal plane wedging in the vertebrae and discs of the growing scoliotic spine to investigate scoliosis progression with growth, and to assess whether the theory of progression initiating in the discs held true for a series of AIS patients with mild to moderate right thoracic major curves. We note that the findings of the current study are relevant to a subset (Lenke type 1 curves) of the larger group of AIS phenotypes, and the dominance of this subtype in our study group is typical of clinical experience at our Center.

On the sequential MRI scans that were used to track the deformity, any individual vertebral or disc wedge angle greater than the intraobserver measurement variability of 3.9° was considered a ‘‘real’’ change (as opposed to a potential measurement error). Over the whole patient group, progression occurred in almost half of the intervals in the study, and there was no statistically significant effect of bracing, age, Cobb angle at the start of the interval, or

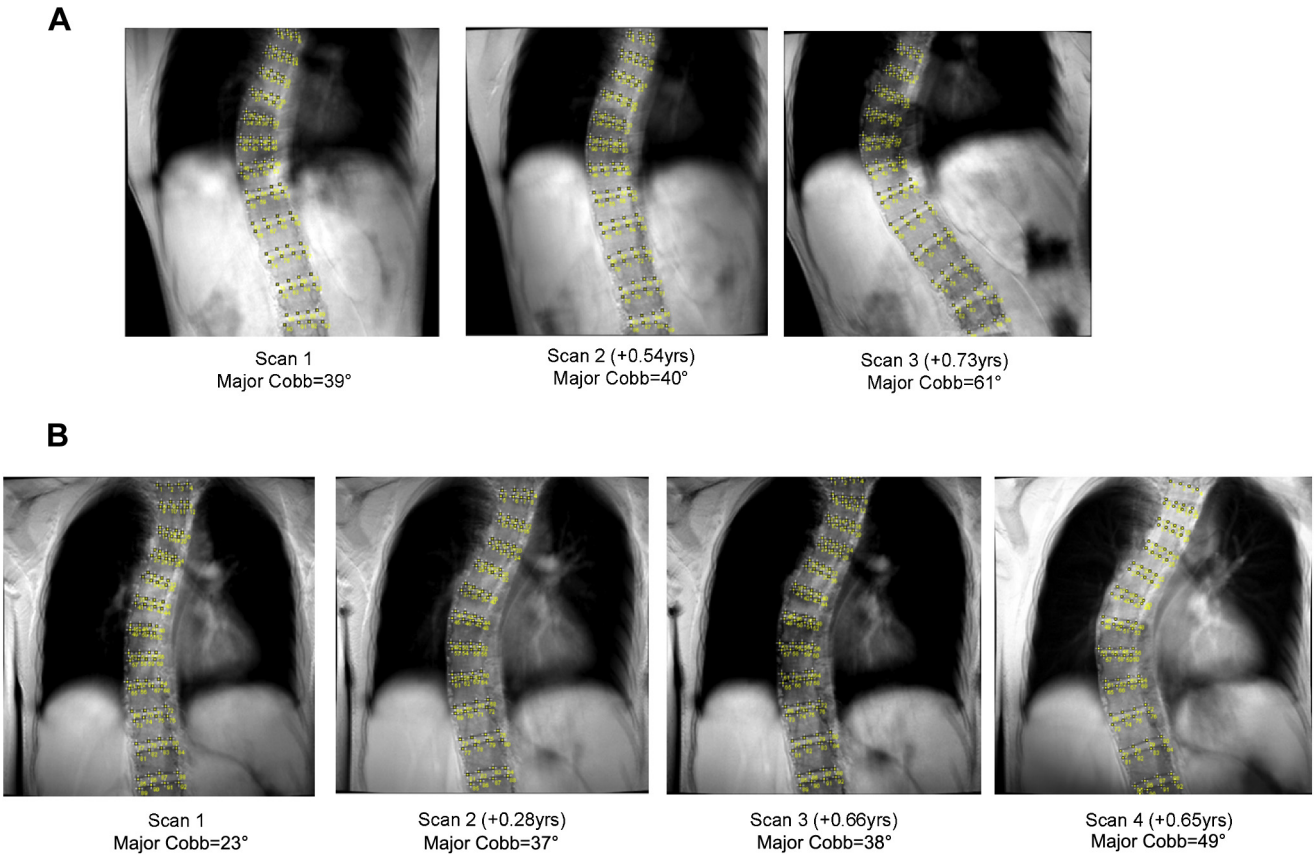

Fig. 7. Coronal plane reconstructions at each scan for (A) Patient 3 and (B) Patient 6, showing the curve progression over time for the two patients who progressed most over the course of the study. The time between each scan and the preceding one is given beside the scan number in each case.

percentage of wedging occurring in the discs (as opposed to in the vertebral bodies) on whether progression occurred or not. The only statistically significant predictor of progression over an interval was interval length, although we stress that with n = 16 the lack of significant correlation with other candidate independent variables should not be regarded as definitive.

We hypothesized that there would be a consistent pattern of increasing coronal plane deformity in the vertebrae and discs with curve progression during growth, and that this pattern would differ between patients whose deformity progresses and those whose did not. However, this hypothesis was not borne out by the results of the study. Looking at the patterns of progression for each patient (Table 5), we saw variable and complex patterns. Counterintuitive findings occurred, such as substantial local anatomic changes to the vertebrae and discs in patients whose overall clinical Cobb angle had not increased. In particular, the vertebral and disc wedge changes across intervals in Table 3 reveal that small overall Cobb changes can mask large changes in disc and bone wedging that are opposite in sign. For example, Patient 15's Cobb angle increased by only 4° between Scans 1 and 2 (therefore not meeting the 5° definition of progression), but this was composed of a large (21°) increase in disc wedging and an 18° decrease in wedging in the vertebral bodies. Such changes in composition of the scoliotic curve during growth are not visible when only considering the overall Cobb angle. There was also no consistent pattern between patients who progressed and those who did not, with some patients (eg, Patient 6 in Fig. 6 starting with a high proportion of deformity in the vertebral bodies and then progressing) and others (eg, Patient 4 in Fig. 6) starting with >50% of the deformity in the discs and then progressing. Of the patients who did not progress, some had deformity primarily in the discs while for others the existing deformity was primarily in the vertebrae (eg, compare Patients 11 and 14 in Fig. 6). With regard to the hypothesis of an increasing proportion of deformity occurring in the vertebrae with curve progression, as presented in Section 3.3 this only occurred for 4 of the 16 patients in the study, and the latter two of these patients (12 and 16) did not undergo clinically significant progression. However, as already acknowledged, we are aware that the sample size in this study is modest, and therefore patterns may emerge when analyzing a larger cohort.

With regard to proportions of wedging above and below the apex of the major curve, we found there was almost twice as much wedging in the discs above the apex than below. Conversely, there was equal wedging in the vertebral

bodies above or below the apex; therefore, the overall Cobb angle was divided roughly 60/40 above and below the apical vertebra.

With regard to growth and deformity progression, although some participants grew 10 cm or more over the course of the study, there was no clear relation between growth velocity and Cobb progression. For example, Table 4 shows intervals for which participants' growth velocity was ~1 cm/month (Patients 5, 15, and 16) during which no clinically significant Cobb progression occurred, and other intervals with relatively slow growth velocity of 0–0.3 cm/month (Patient 3 intervals 1–3 and 2–3, and Patient 6 interval 2–4) during which rapid Cobb progression occurred. Having said this, it is important to keep in mind that standing height growth includes both leg and trunk growth, and secondly that when patients' deformities are progressing rapidly this may reduce their apparent height growth velocity because of the lateral component of spine displacement.

A previous study by Modi et al. found that in curves less than 30°, the average coronal plane wedging at the apex was 2.7° in the vertebral body and 2.1° at the disc, increasing to 4.1° and 3.6° (vertebra and disc), respectively, with curves greater than 30° [8]. By comparison, we found similar apical vertebra wedge angles of 2.8° in curves less than 30° and 6.3° in curves greater than or equal to 30°. As the apex was always chosen to be a vertebra, the disc wedge values reported here are mean values for the two IVDs immediately above and below the apical vertebra, such that for curves $<30°$ the mean apical disc wedging was 1.7°, increasing to 3.4° for curves $\geqslant 30°$.

With regard to the occurrence of negative or reverse wedging at individual spinal levels (refer to Fig. 2 and Table 5), while negative wedging occurred in ~20% of the individual-level measurements in the study, large negative wedge angles (greater than the 3.9° measurement limit) were rare, occurring in only 8/604 individual-level measurements. Furthermore, none of these large negative wedge angles persisted across two or more scans. To date, the authors are aware of only one paper in the literature that presented data showing reversal of vertebra or disc wedge angles over time. However, the authors made no comment on these reversals [6]. It is possible that reverse wedging that occurred toward the limits of the major curve in the present study (ie, Patients 3, 5, 10, and 13) could have been due to a change in sign of the disc wedging occurring within the limits of the major curve (since Cobb is defined according to vertebral body extents rather than discs); however, we note that substantial reverse wedging also occurred at levels well within the major curve in Patients 14 and 15.

Specifically looking at the two patients who underwent the greatest progression over the duration of the study (Patients 3 and 6, with 22° and 27° progression, respectively, see Fig. 7), we note firstly that both of these patients were braced. Fig. 6 shows the differing progression rates over the intervals between scans for these patients. Patient 3 displays non-progression during the first six months (Cobb remains at ~40°) and then rapid progression during the following eight months (Cobb angle change of 40 to 60°). When considering the location of the deformity in Patient 3, 47% of the wedging occurred in the discs on Scan 1, reduced to only 19% wedging at Scan 2 and then increasing again to 58% at Scan 3 (Fig. 6). Table 3 shows that the lack of progression between Scans 1 and 2 masks a 10° decrease in disc wedging countered by a 12° increase in vertebral body wedging over this interval. Furthermore, if the individual level contributions in the major curve are examined for this patient (Table 5), there were large positive wedge angles (outside the 95% intra-observer variability limits of agreement of ±3.9°) at a number of levels within the major curve, of note being the strong increase in disc wedging near the apex at the third scan (Cobb angle 61° with T6–T7, T7–T8, and T8–T9 discs accounting for 32° of this). Patient 6 underwent gradual progression during the first 3 months (Cobb increase of 14°), no progression during the following eight months and then a Cobb angle increase of 11° eight months later. When considering the location of the deformity in Patient 6, only 5% of the wedging occurred in the discs at Scan 1, increasing to 42% at Scan 2, before reducing again to 30% at Scan 3 and 21% at Scan 4. Therefore, this patient started with almost all the wedging in the vertebrae, underwent initial progression, which was solely in the discs, stabilized for ~8 months and then underwent subsequent progression with increased wedging in the vertebral bodies. Furthermore, when examining the individual-level contributions for this patient in the major curve (Table 5), there were some small negative wedge angles in the discs at all four scans, but none greater than the 3.9° measurement variability.

This study had several limitations. First, we analysed individual vertebra and disc wedge angle changes in the coronal plane only. We acknowledge that this only provides a partial picture of the 3D deformity progression; however, it allows direct comparison with clinically performed coronal plane radiographs which are the current gold standard for AIS assessment in spine clinics worldwide. Future analyses of this sequential MRI data set will take full advantage of the 3D MRI protocol in assessing individual vertebral and disc deformity. It may also be of interest to explore the spine's response to bracing or investigate vertebral levels outside the major curve, but these were beyond the scope of the present study. MRI acquisition volumes are limited when submillimeter resolution settings are used as in the current study, such that it is not possible to capture the entire thoracolumbar spine in a single acquisition while also maintaining a reasonable scan time.

Furthermore, the MRI scans in this study were performed in the supine position, which alters the geometry of the spine, because of a shift in applied gravitational loading compared to standing, which will have an effect on the

contribution of the discs to the supine-imaged deformity. Prior studies have shown that this change in curve magnitude between supine and standing is known to be 7° to 11° (smaller in supine); therefore, the major Cobb angles reported here would be ~10° greater for the same patients in the standing position, with the difference being due to disc wedging under the effect of gravity. The supine position is useful, however, in some respects, firstly because the spine is imaged in an 'unloaded' position (relative to the axial gravitational load acting in standing), and also because the change in Cobb angle from supine to standing (as used for clinical radiographs) provides an indication of spinal flexibility (deformation under gravitational loading). It may be possible for future studies to perform this type of research using an upright imaging modality such as EOS or open magnet MRI; however, the relatively high resolution (3D acquisition with 0.5 mm voxel size) achieved in the present study would not be achievable in existing open magnet standing MR scanners.

The time interval between scans in this study was chosen according to each patient's remaining growth potential. Since the patients were recruited to the study at different points in their adolescent growth phase and had differing severities of scoliosis, the interval between scans was adjusted such that those patients considered to be at low risk of rapid growth, and therefore progression, were given a longer time interval. Growth velocity charts in existing literature show that female patients who are skeletally immature (Risser 0) and 11 years of age will grow approximately 10 cm in trunk height before the age of 13 [16]. Following this stage, the amount of remaining growth reduces over 2.5 years until the patient reaches skeletal maturity at Risser 5. It is also known that spines with Cobb angles greater than 30° are at high risk of long-term progression regardless of skeletal maturity status [17-19], and this was also taken into account in prescribing time intervals between scans. Because recruitment of patients to the study depended on them attending the hospital spine clinic with a pre-existing deformity, it was not possible to standardize either starting age or deformity severity; however, the data collected reflect the demographics of patients in a typical deformity clinic.

Conclusions

Sequential MR imaging of scoliosis patients with mild and moderate deformities during growth revealed complex patterns of coronal plane wedging in individual vertebrae and discs. In particular, measurable wedging changes at individual levels can cancel each other out because of reverse wedging, so that the overall Cobb angle of the major curve does not change. There was no clear trend for wedging to commence in the discs and then transfer to the vertebral bodies during subsequent progression as has been previously suggested, and changes in the proportion of wedging between vertebrae and discs which occurred in one growth interval are sometimes reversed during a subsequent growth interval. This work will be extended to three-dimensional analysis of a larger MRI data set in future studies. The clinical significance of the present study is that use of the Cobb angle for tracking deformity severity can mask potentially important changes in the deformity that are occurring at the level of individual vertebrae and discs.

References

[1] Cobb J. Outline for the study of scoliosis. *Instr Course Lect Am Acad Orthop Surg* 1948;5:261–75.

[2] Schick D. *Computed tomography radiation doses for paediatric scoliosis scans*. Unpublished internal report commissioned by Paediatric Spine Research Group from Queensland Health Biomedical Technology Services, Brisbane, Australia, 2004.

[3] Pace N, Ricci L, Negrini S. A comparison approach to explain risks related to x-ray imaging for scoliosis, 2012 SOSORT award winner. *Scoliosis* 2013;8:11.

[4] Presciutti SM, Karukanda T, Lee M. Management decisions for adolescent idiopathic scoliosis significantly affect patient radiation exposure. *Spine J* 2014;14:1984–90.

[5] Levy AR, Goldberg MS, Mayo NE, et al. Reducing the lifetime risk of cancer from spinal radiographs among people with adolescent idiopathic scoliosis. *Spine* 1996;21:1540–7.

[6] Stokes IA, Aronsson DD. Disc and vertebral wedging in patients with progressive scoliosis. *J Spinal Disord* 2001;14:317–22.

[7] Scherrer SA, Begon M, Leardini A, et al. Three-dimensional vertebral wedging in mild and moderate adolescent idiopathic scoliosis. *PLoS One* 2013;8:e71504.

[8] Modi HN, Suh SW, Song HR, et al. Differential wedging of vertebral body and intervertebral disc in thoracic and lumbar spine in adolescent idiopathic scoliosis—a cross sectional study in 150 patients. *Scoliosis* 2008;3:11.

[9] Clin J, Aubin C-É, Lalonde N, et al. A new method to include the gravitational forces in a finite element model of the scoliotic spine. *Med Biol Eng Comput* 2011;49:967–77.

[10] Will RE, Stokes IA, Qiu X, et al. Cobb angle progression in adolescent scoliosis begins at the intervertebral disc. *Spine* 2009;34:2782–6.

[11] Taylor TK, Ghosh P, Bushell GR. The contribution of the intervertebral disk to the scoliotic deformity. *Clin Orthop Relat Res* 1981: 79–90.

[12] Risser JC. The Iliac apophysis; an invaluable sign in the management of scoliosis. *Clin Orthop Relat Res* 1958;11:111–9.

[13] Keenan BE, Izatt MT, Askin GN, et al. Segmental torso masses in adolescent idiopathic scoliosis. *Clin Biomech (Bristol, Avon)* 2014;29:773–9.

[14] Schmitz A, Konig R, Kandyba J, et al. Visualisation of the brace effect on the spinal profile in idiopathic scoliosis. *Eur Spine J* 2005;14: 138–43.

[15] Lenke LG, Betz RR, Harms J, et al. Adolescent idiopathic scoliosis: a new classification to determine extent of spinal arthrodesis. *J Bone Joint Surg Am* 2001;83:1169–81.

[16] Charles YP, Dimeglio A, Canavese F, Daures JP. Skeletal age assessment from the olecranon for idiopathic scoliosis at Risser grade 0. *J Bone Joint Surg Am* 2007;89:2737–44.

[17] Tan KJ, Moe MM, Vaithinathan R, Wong HK. Curve progression in idiopathic scoliosis: follow-up study to skeletal maturity. *Spine* 2009;34:697–700.

[18] Soucacos PN, Zacharis K, Gelalis J, et al. Assessment of curve progression in idiopathic scoliosis. *Eur Spine J* 1998;7:270–7.

[19] Weinstein SL, Ponseti IV. Curve progression in idiopathic scoliosis. *J Bone Joint Surg Am* 1983;65:447–55.